ESR and ENDOR Spectroscopy of Solitons and Polarons in π-Conjugated Polymers

Shin-ichi Kuroda

Department of Applied Physics, Graduate School of Engineering, Nagoya University, Chikusa-ku, Nagoya 464-8603, Japan

Fax: 81-52-789-3712, e-mail: kuroda@nuap.nagoya-u.ac.jp

Nonlinear excitations such as solitons and polarons in conjugated polymers carry spins. In this case, electron spin resonance (ESR) and electron-nuclear double-resonance (ENDOR) provide unique methods to determine their wave function. In this review article, the case of solitons in polyacetylene, CH_x, and polarons in an electroluminescence polymer, poly(paraphenylene vinylene) (PPV) are discussed as typical examples. High-resolution proton ENDOR spectra, obtained with stretch-oriented samples, yield the half extension of 18 carbon atoms for CH_x and 4 phenyl rings for PPV. These extensions are well described by the theories in the case of finite electron correlation. In addition, light-induced ESR technique is shown to be useful in obtaining site-selective information of spin distribution in the case of PPV derivatives, as well as the excitation spectra of polarons. New examples are highly electroluminescent phenyl-substituted PPV and composites of fullerene and regioregular poly(3-alkylthiophene), RR-P3AT, or polyfluorene. In the case of RR-P3AT/C_{60}, light-induced ENDOR (LENDOR) has also been successful in obtaining polaron extension.

Key words: electron spin resonance, electron-nuclear double-resonance, π-conjugated polymers, solitons, polarons

1. INTRODUCTION

Since the discovery of metallic conductivity in doped polyacetylene films, many conjugated polymers have been synthesized to develop conducting polymers [1,2]. In addition, another important property of conjugated polymers has been added in 1990, when intense electroluminescence has been discovered in a polymer, poly(paraphenylene vinylene) (PPV), and its derivatives [3]. Now the displays with light-emitting polymers are approaching to the threshold of commercial application [4]. More recently, the successful synthesis of region-regular polyalkylthiophene has made possible to make well ordered structure of the polymer chains due to self organization, which resulted in the drastic increase of the carrier mobility of field-effect-transistors (FET), fabricated, for example, by ink-jet printing [5]. These conjugated polymers, at the same time, attract much attention as one-dimensional electronic systems that can generate nonlinear excitations such as solitons and polarons [2]. These excitations give rise to characteristic absorptions in optical, magnetic and other spectroscopic measurements.

In this review article, I discuss the application of electron spin resonance (ESR) and electron-nuclear double-resonance (ENDOR) spectroscopies of proton on the conjugated 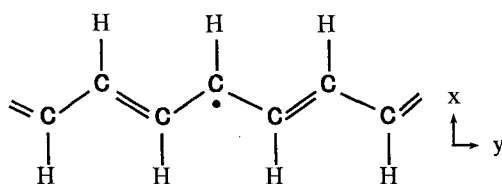chain to directly measure the spin density distribution of paramagnetic excitations through the study of hyperfine coupling [6-10].

2. SOLITONS IN POLYACETYLENE

The chemical structure of *trans*-polyacetylene containing a soliton at the center is shown in Fig. 1. In Figs. 1 and 2, is also shown the definition of the coordinate axes in this paper, where the x and y axes are parallel to the C-H bond axis and the pπ orbital axis, respectively. A finite spin density ρ on a carbon pπ orbital gives rise to a hyperfine coupling with the proton bonded to the carbon with the magnitude of ρA. Here **A** is the hyperfine tensor of a π-electron due to the C-H proton. The tensor becomes diagonal in the above coordinate system and the principal components are given as

$$A_{xx} = -(1-\alpha)A, \qquad A_{yy} = -(1+\alpha)A, \qquad A_{zz} = -A. \qquad (1)$$

Here A is so called McConnell constant, having the magnitude of 56-84 MHz in the frequency units. We adopt a typical value of A = 70 MHz in the subsequent
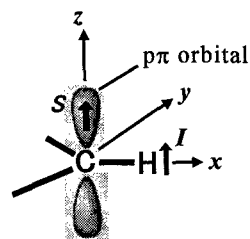

Fig. 2. pπ orbital of a carbon atom bonded to a proton in conjugated structure. Coordinate axes are also shown. These axes become principal axes of g and hyperfine tensors of a π electron.
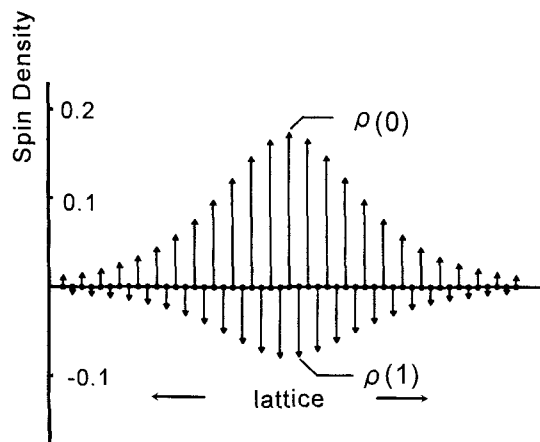

Fig. 1. Solitons in *trans*-polyacetylene. Coordinate axes are also defined.

Fig. 3. Spin density distribution of the soliton in the case of the finite electron correlation.

ENDOR FREQUENCY (MHz)

Fig. 4. Detailed comparison of the frequency-derivative ENDOR spectra of a stretch-oriented *cis*-rich polyacetylene for the ν_+ branch ($\nu > \nu_p$). The external field is parallel and perpendicular to the stretch direction of the sample for the thick- and thin-lines, respectively. Dashed arrows show the frequencies corresponding to the hyperfine tensor components as indicated.

analysis. $\alpha \sim 0.5$ represents the relative magnitude of the anisotropic coupling. Among the three tensor components, A_{yy} has the largest absolute magnitude. The *y*-axis becomes the chain axis in *trans*-polyacetylene.

The ENDOR frequencies of a proton bonded to a carbon with spin density ρ on its $p\pi$ orbital are expressed for the principal axes, as follows,

$$\nu_\pm = \left| \nu_p \pm \frac{1}{2}\rho A_{ii} \right|, \quad \text{for } i = x, y, z \quad (2)$$

where $\pm$ represent the two branches of the ENDOR frequency and ν_p is the free proton frequency. A_{ii} shows the principal hyperfine tensor components given by Eq. (1). The second term of the right hand side shows the frequency shift due to the hyperfine field and $\pm$ sign corresponds to up and down electron-spin orientation. Thus the spin density of the *n*-th carbon site from the center of the soliton is directly observed as the ENDOR frequency shift $(1/2)\rho(n)A_{ii}$, giving the form of spin distribution. The ENDOR signal, however, is not always detectable due to signal-to-noise ratio limitation, then dark or light-induced ESR spectra also provide an equally important alternative method to study spin distribution, through the ESR spectrum simulation method that calculates the hyperfine splittings of the paramagnetic center based on the anisotropic g and hyperfine tensors of π-electron. Recent typical example is demonstrated when the hyperfine ESR linewidth is significantly modified due to the substitution of protons by other groups, as to be discussed in Sect. 3.

Thus the hyperfine coupling of π-electron given in Eq. (1) plays a crucial role in obtaining the spin density from the observed ENDOR spectra determined by Eq. (2). Then the verification of the π-electron character of spins becomes an important prerequisite when one is engaged in the ENDOR of paramagnetic excitations in the π-electron system of conjugated polymers. In the case of polyacetylene and PPV, verification is adequately done by confirming π-electron anistotropy of ESR and ENDOR spectra using stretch-oriented polymers where the molecular axes are preferentially oriented.

Figure 3 shows schematically the spin density distribution of the soliton in the case of finite electron correlation. The filled circles of abscissa represent individual carbon site. The full width at half maximum
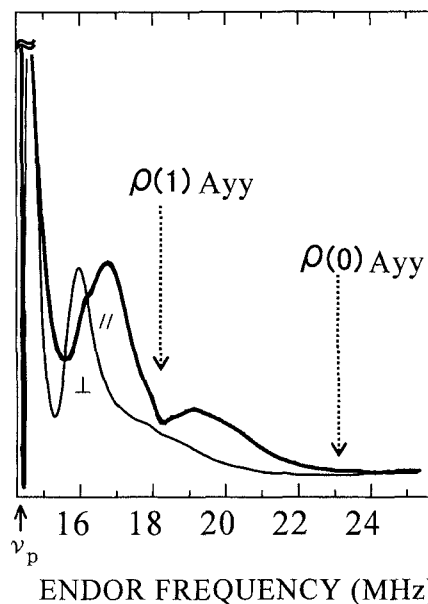
of the spin density of 18 carbon atoms is shown in Fig. 3. As discussed below, the extension is directly obtained from the observed maximum ENDOR frequency. The negative spins arise from the effect of finite electron correlation. In the original Su-Schrieffer-Heeger model, where the electron correlation is neglected, the unpaired electron density appears at each even carbon site from the center of the soliton. On the other hand, in the case of finite electron correlation, spin polarization due to correlation occurs and negative spins are induced at odd carbon sites. Its magnitude directly provides the strength of the electron correlation energy of the system. Such occurrence of negative spin sites can be recognized as the spectral turning points resolved for the ENDOR spectrum of the stretch direction, as explained below.

Figure 4 shows the anisotropy of the frequency-derivative ENDOR spectra at 12K in a 190% stretched *cis*-rich polyacetylene for ν_+ branch ($\nu > \nu_p$). In the *cis*-rich sample, the short average length of *trans*-segments in the *cis*-matrix restricts the motion of the soliton at low temperatures, which is suitable for the measurement of the spin distribution obtained from the static hyperfine couplings of the soliton [6,7,9,10]. In Fig. 4, thick lines and thin lines show the spectra with the external magnetic field parallel and perpendicular to the stretch direction, respectively. The larger ENDOR shift observed for the stretch direction is the direct consequence of the π-electron nature of the soliton, since the y-axis component of the hyperfine tensor with the largest magnitude should be observed preferentially for the stretch direction. The most important quantity determined from the spectra is the maximum ENDOR shift in the stretch direction, that is, $(1/2)\rho(0)A_{yy}$, which can be accurately determined from the wing of the
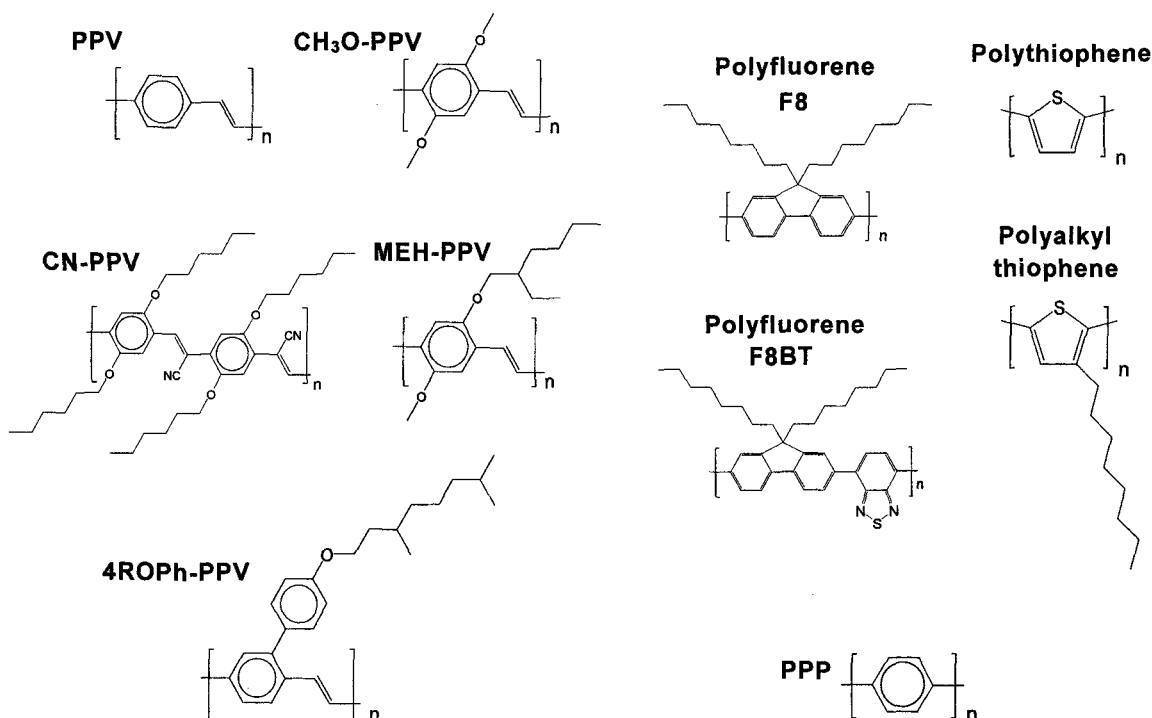
Fig. 5.   Chemical structures of various π-conjugated polymers.

spectra using ENDOR-induced ESR technique, and $\rho(0)$ = 0.17 has been obtained. On the other hand, the spectral turning point can be shown to associated with the negative spin sites with smaller peak density of ρ (± 1), as in Fig. 3. Its value has been obtained as ρ (± 1) = -0.075 and then ρ (± 1)/ ρ (0) = -0.44. The negative sign has been actually confirmed by electron-nuclear-nuclear triple (TRIPLE) resonance technique. More details are described elsewhere [9,10].

The functional form of the spin density distribution by the soliton theory for finite electron correlation is characterized by the *sech*-form. Then the bound condition for the total sum of the spin densities to be unity yields the extension of the soliton to be 18 carbon atoms. These observed results are well reproduced theoretically by Yonemitsu et al. with on-site and near-neighbor Coulomb interaction of $U = 1.6t_0$, $V = 0.8$ t_0 where t_0 designates the transfer integral. Similar results as those in *cis*-rich Shirakawa samples, *i.e.*, the similar spectra with resolved structures for the stretch-direction and similar spectral frequencies have been reported for stretch-oriented *trans*-polyacetylene prepared by the Durham route, where the unpaired electrons observed were conjectured to be trapped solitons form nearly temperature-independent ENDOR spectra [2]. Discussion of this as well as other systems can be found elsewhere [9,10].

3. POLARONS IN PPV AND ITS DERIVATIVES

Figure 5 shows the chemical structures of various π-conjugated polymers besides *trans*-polyacetylene. In *trans*-polyacetylene, the structure is so-called degenerate and soliton becomes the primary nonlinear excitation. On the other hand, most of other conjugated polymers are structurally nondegenerate and solitons can not exist. In this case, polarons with spin and charge are considered to be charge carriers in most of polymer used in electronic devices such as electroluminescent (EL) displays,

thin-film-transistor, solar cells, etc. Thus the studies of polarons in various polymers are of fundamental importance in understanding basic physical processes involved in these devices and improving efficiencies.

In Fig. 5, the left-hand side mainly show PPV families, for example, typical soluble polymers such as MEH-PPV and more recently a highly-electroluminescent phenyl-substituted 4ROPh-PPV. The middle row show recent important polymer, polyfluorene and a co-polymer derivative, which are used for actual multi-color EL device proto-types. The right-hand side show the typical hetero-atom containing conjugated polymer, polythiophene (PT) and its soluble analog polyalkylthiophene (PAT) where recently developed region-regular PAT's show high carrier mobility owing to their highly self-organized molecular order. At the right-hand bottom, is also shown another important polymer polyparaphenylene (PPP).

3.1 Polaron spin distribution in PPV determined by ENDOR

Figure 6 shows schematically the plus- and minus-charged polarons, P^+ and P^-, that are created by adding a hole or an electron to the nondegenerate polymer structure, PPV in this case. As a result of addition of $\pm$ charges polarons are created with schematic structure associated with energetically higher quinoid structure obtained by exchanging the single and double bonds of normal phenylene-vinylene structure. Both ends of this energetically higher structure region are terminated by a neutral ($\bullet$) and a charged ($\pm$) solitons. In other words, the polaron can be viewed as a bound pair of two solitons, one charged and the other, neutral [2]. Thus the extension of the polaron would be generally expected to be larger than that of the soliton. This can be seen in actual examples.s In the case of PPV, spins are present in the dark state of the polymer. These dark spins may be
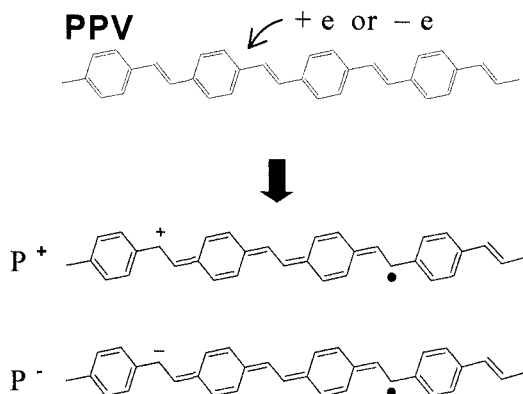
PPV + e or – e

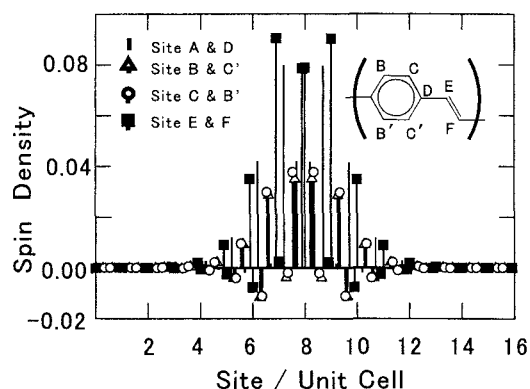

Fig. 6.   Polarons in poly(paraphenylene vinylene)

Fig. 7.   Spin density distribution of a polaron in the PPV chain calculated by PPP model. Vinyl sites (sites E and F) are marked by the solid squares.

trapped polarons from the resemblance between the dark and light-induced ESR (LESR) signals, because the latter signals can be associated with ± polarons generated by photoinduced charge transfer in the system. ESR spectra of stretch-oriented samples show the anisotropy consistent with that of π-electrons, qualitatively similar as in the case of stretched polyacetylene films, by taking into account two inequivalent C-H bond orientations for PPV. Proton ENDOR spectra of these trapped polarons have been successfully obtained at 4K in 10 times stretched polymer and the results have been well reproduced by theoretically calculated spin distributions in the case of finite electron-electron interactions.

Figure 7 shows the theoretically calculated spin density distribution of a polaron with PPP (Parise-Parr-Pople) Hamiltonian that explains the observed ENDOR spectra [8-11]. The half width of distribution amounts to about 4 phenyl rings. As for the parameter values of the PPP Hamiltonian used for the result in Fig. 7, they are on-site and nearest-neighbor Coulomb interactions of $U = 2.5t$ and $V = 1.3t$, respectively, with t being transfer integral, and more long-range interactions given by Ohno formula. These values are fairly close to those in the case of solitons in polyacetylene and PPV fall in intermediate coupling regime. An important feature of the spin distribution shown in Fig. 7 is that it consists of three distinct groups in magnitude of spin densities. In particular, the largest group containing the largest and second largest densities of 0.09 and 0.08, respectively, reside on the carbons of vinyl sites, as indicated by solid squares in Fig. 7. This quantity is inversely proportional to the extension of the polaron. It would be quite interesting if we can confirm that the largest densities reside on vinyl sites. In fact, such site-selective information could be obtained by our recent LESR studies of PPV derivatives with different substituent groups for vinyl sites, that is, CN-PPV and MEH-PPV, as described below.

3.2 LESR studies of PPV and its derivatives
3.2.1 Site–selective information on spin distribution of polarons from LESR of MEH-PPV and CN-PPV

LESR is a clean method to observe ± polarons generated by photoinduced charge transfer in conjugated chains. In PPV, anisotropic LESR spectra in stretched samples have been well reproduced by the ESR spectrum simulation method using the above described theoretical spin distribution of a polaron [12]. In Fig. 5 are shown the chemical structures of poly(2-methoxy-5-(2'-ethyl)-

hexyloxy-p-phenylene vinylene), MEH-PPV, and a similar dialkoxy derivative, CN-PPV, where cyano groups are attached to the carbons of vinyl sites instead of half of protons (see Fig. 5). According to the above obtained spin distribution of the polaron in PPV, maximum spin densities reside on the vinyl sites. In this case, it should be expected that the hyperfine contribution to the ESR linewidth should be drastically decreased due to the loss of significant vinyl proton hyperfine splitting due CN substitution without nuclear spins.

Such situation has been actually confirmed. LESR signals have been successfully detected for both polymers with almost negligible dark ESR signals. Full width at half maximum of the integrated form of these spectra are 6.6 ± 0.2 and 4.5 ± 0.1G for MEH-PPV and CN-PPV, respectively. This fact alone shows that the hyperfine width of CN-PPV is significantly reduced compared with the case of MEH-PPV. The results are also consistent with previous optically detected magnetic resonance (ODMR) studies of the polaron signals in PPV and CN-PPV, where a considerable reduction of ESR linewidth was observed for CN-PPV compared with PPV [15]. Since CN-PPV has not only substitution by CN groups but also by alkoxy groups at phenyl rings of PPV, the effect of CN substitution can be identified uniquely by the present comparison of CN-PPV and MEH-PPV, both of which have similar alkoxy substitution at the same sites on the phenyl rings. The LESR liewidths in these polymers can be calculated by using the theoretical spin distribution of the polaron previously obtained for PPV by ENDOR. Calculated widths are 6.1G and 4.9G in MEH-PPV and CN-PPV, respectively, in reasonable agreement with the observed widths.

3.2.2 Excitation spectra of polarons in PPV derivatives
The excitation spectrum of the LESR signal provides important information concerning the mechanism of the charge separation. The top and middle curves in Fig. 8 show the variation of the normalized LESR intensity with the photon energy of incident light in MEH-PPV and CN-PPV films. The light intensity was adjusted to give the same photon flux at each wavelength. The solid line in each figure shows the optical absorption spectrum. It is seen that the LESR intensity becomes large at high excitation energies, as observed in PPV. The distinct feature of the present case is that the action spectrum has a clear threshold at an energy of 2.7-2.8 eV in CN-PPV
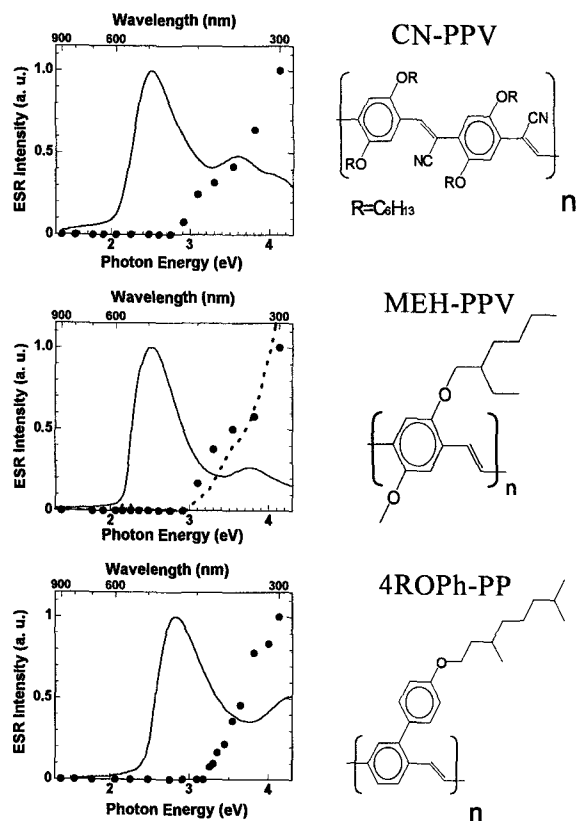
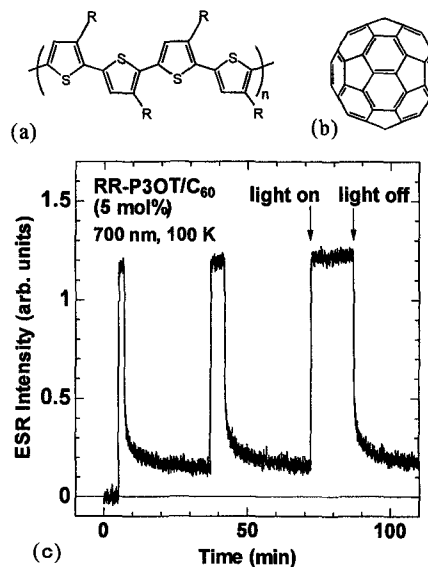Fig. 8. Excitation spectra of LESR for CN-PPV, MEH-PPV and 4ROPh-PPV.

Fig. 9. Upper figures: Chemical structure of (a) regioregular poly(3-alkylthiophene) and (b) fullerene. Lower figure: Transient response of the LESR intensity of the RR-P3OT/C_{60} composite (5 mol%) upon irradiation by repeated light (700 nm) pulses with different time widths. The data were recorded using the lower field peak of the RR-P3OT signal (g_{PAT}) at 100K.

and around 3 eV in MEH-PPV, which is higher than the threshold energy of optical absorption of about 2.5 eV in both polymers. The threshold energy of the LESR action spectrum can be related to the band-gap energy. It should be pointed out that the complete absence of LESR signals around the optical absorption peak is not always realized in all kinds of conjugated electroluminescent polymers, which could be related to, for example, the effect of defects or higher-order structure such as aggregation of polymer chains. But even in this case, a steep rise can be observed around 3 eV for PPV's and the LESR intensity would reflect the efficiency of the charge separation. A similar phenomenon with a clear threshold for the LESR action spectrum, as the above two examples is observed in the case of phenyl-substituted PPV, that is 4ROPh-PPV as shown at the bottom of Fig. 8. In this case, the peak energy of the optical absorption of about 2.8 eV is small but definitely larger than that of about of 2.5 eV for the above two polymers. Correspondingly, the threshold energy of the LESR action spectrum is shifted for the higher-energy side and becomes about 3.2 eV. Thus the difference of the optical peak and the threshold energy is similar among those polymers shown here. The last polymer attracts attention because of its high electroluminescence efficiency among PPV families [16]. The origin of the high efficiency, brought about by only the phenyl substitution, is an interesting problem. ESR and ENDOR spectra of this polymer, compared with other polymers, might provide useful information on this problem and such studies are currently in progress. Preliminary results show an interesting self-organized spontaneous molecular preferential orientation along the

normal direction of the substrate of cast films. Further studies are currently under progress.

It is interesting to note that a similar behavior with a distinct threshold around 3 eV is reported in the action spectrum of photoconductivity in MEH-PPV, as indicated by the dotted line in the middle curve in Fig. 8. [17] The observed resemblance between the action spectra of LESR and photoconductivity provides supporting evidence that the photoinduced spins are charged species, that is, polarons.

4. LESR studies of conjugated polymers/C_{60} composites
4.1. LESR and LENDOR studies of regioregular poly(3-alkylthiophene)s (RR-PATs)/ C_{60} composites

Early examples of photoinduced charge transfer in the conjugated polymers/C_{60} composites have been reported for the cases of regio-random PAT [18] and MEH-PPV [19]. We have been recently successful in observing strong LESR in Regioregular poly(3-alkylthiophene)s (RR-PATs)/ C_{60} composites resulting from a remarkable enhancement quantum yield around 700 nm in the LESR action spectrum [20]. Examples of transient response of LESR signals are shown in Fig. 9. Owing to this enhancement, we have been successful in observing the first light-induced ENDOR (LENDOR) of the system as in Fig. 10, which yields the extension of photogenerated polarons of about 10 thiophene rings. More details and analysis of recombination kinetics of photogenerated polarons are described elsewhere [21, 22]

4.2. Polyfluorene/C_{60} composites

It is interesting to note that a similar LESR signals due to photoinduced charge transfer is also observed in polyfluorene/C_{60} composites as shown in Fig. 11. Detailed studies of this system are currently in progress.
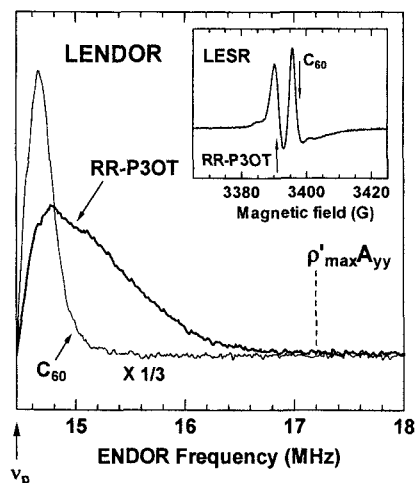
Fig. 10. Frequency-derivative LENDOR spectra of the RR-PAT/C_{60} composite at 4 K under 700 nm (~ 1.8 eV) illumination for the frequency region higher than the free-proton frequency v_p = 14.45 MHz. Thick and thin lines represent the spectra of RR-P3OT and C_{60}, which are obtained by using the resonance-magnetic fields of the LESR signals of positive polarons in RR-P3OT (g = 2.002) and C_{60}^- (g = 1.999) shown by arrows in the inset, respectively. Dashed line represents the maximum ENDOR shift of the RR-P3OT signal corresponding to the maximum hyperfine-tensor component as indicated. Inset: First-derivative LESR spectrum of the RR-PAT/C_{60} composite at 4 K under 700 nm

5. CONCLUSIONS

As described in this review paper, ESR and ENDOR conjugated polymers and conjugated polymer/fullerene composites are useful to study solitons and polarons in conjugated polymers. Further applications would be expected to extend the studies to other important polymers. New detection schemes would be also pursued and we note here the field-induced doping of polymer films using device structures as an new example [23,24].

REFERENCES

[1] H. Shirakawa, E.J. Louis, A.G. MacDiarmid, C.K. Chiang and A.J. Heeger, *J. Chem. Soc. Chem. Comm.*, **1977**, 578-580 (1977).

[2] A.J. Heeger, S. Kievelson, J.R. Schrieffer and W.P. Su, *Rev. Mod. Phys.*, **60**, 781-850 (1988).

[3] J.H. Burroughes, D.D.C. Bradley, A.R. Brown, R.N. Marks, K. Mackay, R.H. Friend, P.L. Burns and A.B. Holms, *Nature*, **347**, 539-541 (1990).
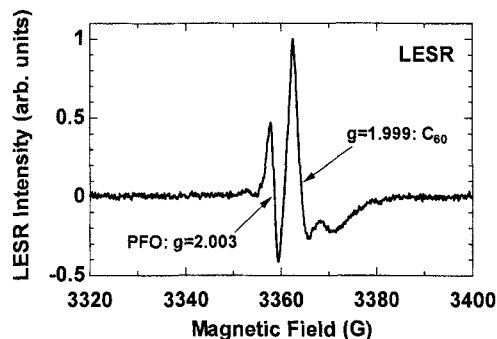

Fig. 11. LESR spectrum of a cast film of polyfluorene/C_{60} composite

[4] R.H. Friend, R.W. Gymer, A.B. Holmes, J.H. Burroughes, R.N. Marks, C. Taliani, D.D.DC. Bradley, D.A. Dos Santos, J.L. Bredas, M. Loegdlund, W.R. Salaneck, *Nature*, **397**, 121-128 (1999).

[5] H. Sirringhaus, P.J. Brown, R.H. Friend, M.M. Nielsen, K. Bechgaard, B.M.M. Langeveld-Voss, A.J.H. Spiering, R.A.J. Janssen, E.W. Meijer, P. Herwig and D. M. de Leeuw, *Nature*, **401**, 685-688 (1999).

[6] S. Kuroda and H. Shirakawa, *Solid State Commun.*, **43**, 591-594 (1984).

[7] S. Kuroda and H. Shirakawa, *Phys. Rev. B*, **35**, 9380-9382 (1987).

[8] S. Kuroda, T. Noguchi and T. Ohnishi, *Phys. Rev. Lett.*, **72**, 286-289 (1994)

[9] S. Kuroda, *Int. J. Mod. Phys. B*, **9**, 221-260 (1995).

[10] S. Kuroda, *Appl. Magn. Reson.*, **23**, 455-468 (2003)

[11] Y. Shimoi, S. Abe, S. Kuroda and K. Murata, *Solid State Commun.*, **95**, 137-141 (1995).

[12] K. Murata, S. Kuroda, Y. Shimoi, S. Abe, T. Noguchi and T. Ohnishi, *J. Phys. Soc. Jpn.*, **65**, 3743-3746 (1996).

[13] K. Murata, Y. Shimoi, S. Abe, S. Kuroda, T. Nobuchi and T. Ohnishi, *Chem. Phys.*, **227**, 191-201 (1998).

[14] S. Kuroda, K. Marumoto, H. Ito, N.C. Greenham, R.H. Friend, Y. Shimoi and S. Abe, *Chem. Phys. Lett.*, **325**, 183-188 (2000).

[15] N.C. Greenham, J. Shinar, J. Partee, P.A. Lane, O. Amir, F. Lu, R.H. Friend, *Phys. Rev. B*, **53**, 13528-13533 (1996).

[16] H. Spreitzer, H. Becker, E. Kluge, W. Kreuder, H. Schenck. R. Demandt and H. Schoo, *Adv. Mater.*, **10**, 1340 (1998)

[17] A. Koehler, D.A. Dos Santos, D. Beljonne Z. Shuai, J.L. Bredas, A.B. Holmes, A. Kraus, K. Muellen and R.H. Friend, *Nature*, **392**, 903-906 (1998).

[18] S. Morita, A.A. Zakhidov and K. Yoshino, *Solid State Commun.*, **82**, 249-252 (1992).

[19] N.S. Sariciftci, L. Smilowitz, A.J. Heeger and F. Wudl, *Science*, **258**, 1474-1476 (1992).

[20] K. Marumoto, N. Takeuchi, T. Ozaki and S. Kuroda, *Synth. Met.*, **129**, 239-247 (2002).

[21] K. Marumoto, N. Takeuchi and S. Kuroda, *Chem. phys. Lett.*, in press.

[22] K. Marumoto, Y. Muramatsu and S. Kuroda, *These Proceedings*.

[23] S. Ukai, H. Ito and S. Kuroda, *Jpn. J. Appl. Phys. Pt.I*, in press.

[24] H. Ito, S. Ukai, N. Nomura, K. Hayashi, T. Ozaki, K. Marumoto and S. Kuroda, *These Proceedings*.